NANO LETTERS
Letter
Cite This: Nano Lett. XXXX, XXX, XXX−XXX
pubs.acs.org/NanoLett

Spin-Selective Transmission in Chiral Folded Metasurfaces

Shengyan Yang,[†,§] Zhe Liu,[†,∥] Sha Hu,[†,§] Ai-Zi Jin,[†,⊥] Haifang Yang,[†,⊥] Shuang Zhang,[*,‡] Junjie Li,[*,†,⊥] and Changzhi Gu[*,†,§]

[†]Beijing National Laboratory for Condensed Matter Physics, Institute of Physics, Chinese Academy of Sciences, Beijing 100190, China

[‡]School of Physics and Astronomy, University of Birmingham, Birmingham B15 2TT, U.K.

[§]School of Physical Sciences, CAS Key Laboratory of Vacuum Physics, University of Chinese Academy of Sciences, Beijing 100049, China

[∥]Niels Bohr Institute, University of Copenhagen, Blegdamsvej 17, DK-2100 Copenhagen, Denmark

[⊥]Songshan Lake Materials Laboratory, Dongguan, Guangdong 523808, China

ABSTRACT: Controlling the spin angular momentum of light (or circular polarization state) plays a crucial role in the modern photonic applications such as optical communication, circular dichroism spectroscopy, and quantum information processing. However, the conventional approaches to manipulate the spin of light require naturally occurring chiral or birefringent materials of bulky sizes due to the weak light−matter interactions. Here we experimentally demonstrate an approach to implement spin-selective transmission in the infrared region based on chiral folded metasurfaces that are capable of transmitting one spin state of light while largely prohibiting the other. Due to the intrinsic chirality of the folded metasurface, a remarkable circular dichroism as large as 0.7 with the maximum transmittance exceeding 92% is experimentally demonstrated. The giant circular dichroism is interpreted within the framework of charge-current multipole expansion. Moreover, the intrinsic chirality can be readily controlled by manipulating the folding angle of the metasurface with respect to the cardinal plane. Benefiting from its strong chirality and spin-dependent transmission characteristics, the proposed folded metasurface may be applied to a range of novel photon-spin selective devices for optical communication technologies and biophotonics.

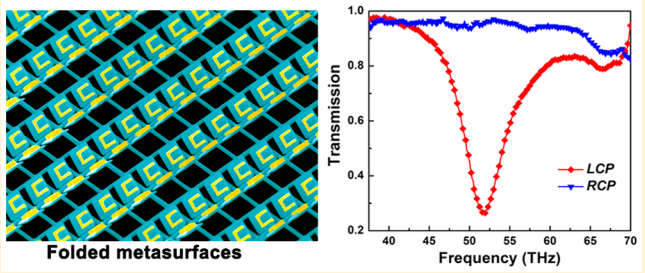

KEYWORDS: *Folded metasurface, intrinsic chirality, subwavelength optics, spin-selective transmission*

It is of critical importance to control the spin angular momentum of light, which is an important degree-of-freedom of photons that is fundamental to many developments in modern physics and applications such as quantum information processing,[1,2] circular dichroism (CD) spectroscopy,[3,4] spin optical communication,[5] molecule imaging and biosensing.[6−8] Natural chiral materials that consist of elements lacking mirror symmetry have been widely used to control the spin states of light.[9,10] However, optical chirality of most natural occurring media, which results in such fundamental polarization effects as in form of optical activity (OA) and associated phenomenon of CD, is extremely small due to the weak chiral matter-light interaction.[8] Therefore, bulky optical elements are usually required to obtain substantial optical chirality, which compromise the polarization modulation efficiency and make it challenging to implement miniature and integrated devices. Moreover, the conventional approach to generate, distinguish, and probe spin of circularly polarized light usually involves multiple optical elements, which are unsuitable for integration in miniaturized optical systems.

Chiral metamaterials, artificial materials that display no mirror symmetry, have enabled the realization of strong chiral optical responses, which play an important role in polarization modulation and spin-optics.[11−42] Light of opposite spins interacts distinctively with chiral metamaterials, resulting in polarization change of the transmitted or reflected light for a linearly polarized incident light. In the past years, there have been a large number of works on 2D metamaterials or metasurfaces with planar chirality, including conjugated gammadion chiral metamaterials,[12−15] fish-scale structures,[16] and many other structures.[17−19] Metasurfaces with extrinsic chirality have also been demonstrated in which the oblique incident electromagnetic wave together with the 2D metasurface forms a 3D configuration that lacks mirror symmetry, such that the interaction between the excited electric and magnetic dipoles results in the external chirality.[20,21] However, chiral optical responses in these existing planar structures are usually small. The realization of the extrinsic chirality requires illumination at oblique angles while the strength of chirality is limited by the incidence angle. In contrast, 3D chiral

Received: November 8, 2018
Revised: December 20, 2018
Published: January 4, 2019

DOI: 10.1021/acs.nanolett.8b04521
Nano Lett. XXXX, XXX, XXX−XXX

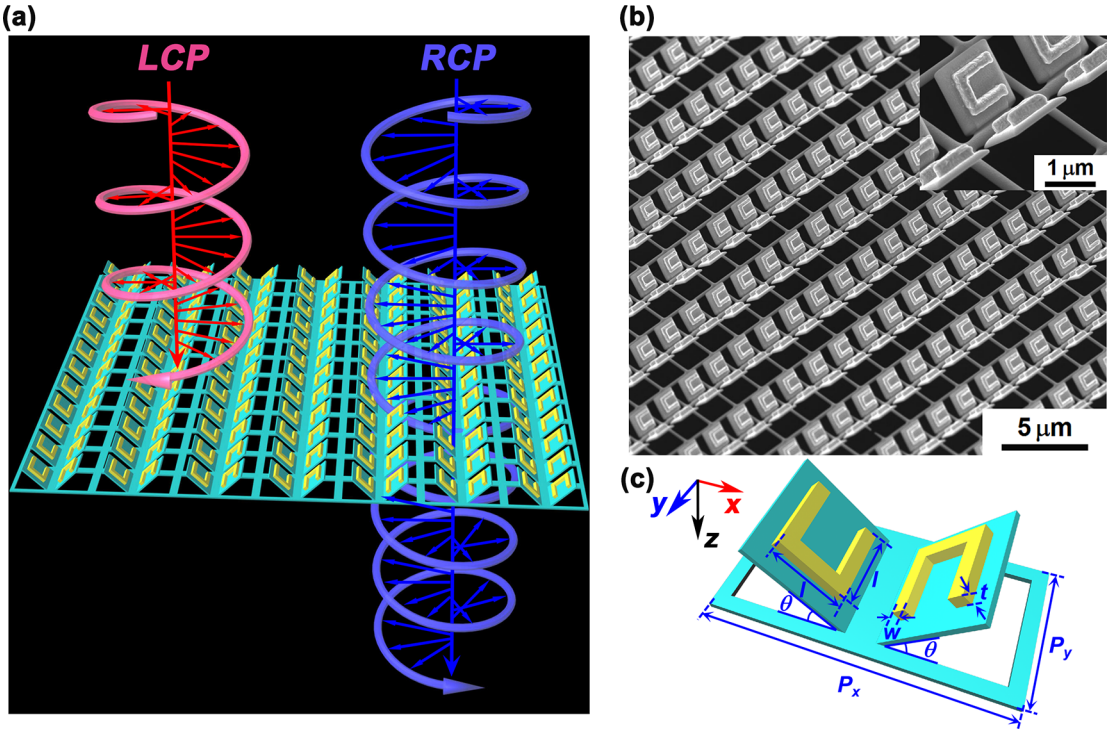

Figure 1. Design of folded metasurface that exhibits spin-resolved optical transmission. (a) Schematic diagram of optical dichroism from the 3D folded metasurface and the illumination configuration. (b) Scanning electron microscope image of the fabricated 3D folded metasurface. Inset: zoomed-in scanning electron microscopy image showing the well-defined structures. (c) Magnified schematic illustrating the composite of a 3D folding metasurface unit cell with labeled dimensions. The parameters are P_x = 4 μm, P_y = 2 μm, l = 900 nm, w = 200 nm, θ = 50°, and t = 200 nm. The thickness of the SiN_x film is 100 nm.

metamaterials possess chiral optical responses significantly stronger than that of their planar counterparts and several orders of magnitude larger than that of the natural materials, which makes 3D chiral metamaterials highly promising candidates for practical applications, such as negative refraction,[22−25] ultrasensitive biosensing,[7] and circular polarizers.[26] There have been some recent progresses in fabricating sophisticated 3D chiral structures that consist of helix architectures or multilayer twisted structures by utilizing direct laser writing,[26,27] focus ion/electron beam deposition[28−30] and multilayer stacking procedures.[31−37] Nevertheless, most of these chiral metamaterials suffer from complicated designs, difficult fabrication processes, insufficient circular dichroism or transmittance, which may hinder their practical applications. Developing a relatively simple, controllable and large-area nanofabrication method for 3D structures exhibiting gigantic intrinsic chirality with deep subwavelength feature sizes remains a challenge. Furthermore, exploring a straightforward strategy for the spin selective transmission may be highly promising in practical applications.

In this letter, we experimentally demonstrate a new approach to realize spin-selective transmission by using a folded metasurface composed of folded antisymmetric split ring resonators (SRRs) that possesses pronounced intrinsic chirality at infrared frequencies. The fundamental design principle is to break the mirror symmetries of the structures by folding the constituent components along a certain angle. The fabrication techniques are based on the combination of electron-beam lithography and focused-ion-beam induced deformation process.[38,39] The giant intrinsic chirality in our proposed folded metasurface originates from the strong coupling of the electric and magnetic dipole resonances hosted by the antisymmetrically folded SRRs as well as contributions from the other electromagnetic multipoles, which consequently lead to efficient spin selective transmission. Moreover, the chirality of the folded metasurface can be effectively modulated by tailoring its geometric configuration, e.g., the folding angle of the SRRs. Compared to conventional 3D chiral metamaterial, this design and fabrication technology does not involve complicated 3D or multilayer fabrication procedures, and thus effectively providing an extra degree of freedom in designing chiral metamaterials for manipulating the spin of light. The concept of folded metasurface may contributes to substantial benefits for many exciting applications in polarization manipulation, spin recognition and selection, chiral sensing, chiral spectroscopy, and imaging.

Results and Discussion. The folded metasurface is evolved from an ordinary planar metasurface consisting of periodically arranged antisymmetric SRRs that possess no intrinsic chirality due to the preserved mirror symmetry. By folding the SRR along the surface normal direction and converting the metasurface into 3D configuration, the mirror symmetry is broken and thus intrinsic chirality is induced. A schematic illustration of the spin-selective transmission in the folded metasurface array is displayed in Figure 1a. The elementary building block of the folded metasurface consists of two antisymmetric SRRs arranged in a 3D configuration via folding the ultrathin silicon nitride (SiN_x) substrate, as illustrated by the unit-cell schematic in Figure 1c. A detailed description of the fabrication procedures of the folded metasurface is provided in the Methods section. The folding angle of the constituent SRR can be well controlled by the incident direction of ion beam respect to the sample surface normal and the dose of the incident ion beam. Figure 1b shows

DOI: 10.1021/acs.nanolett.8b04521
Nano Lett. XXXX, XXX, XXX−XXX

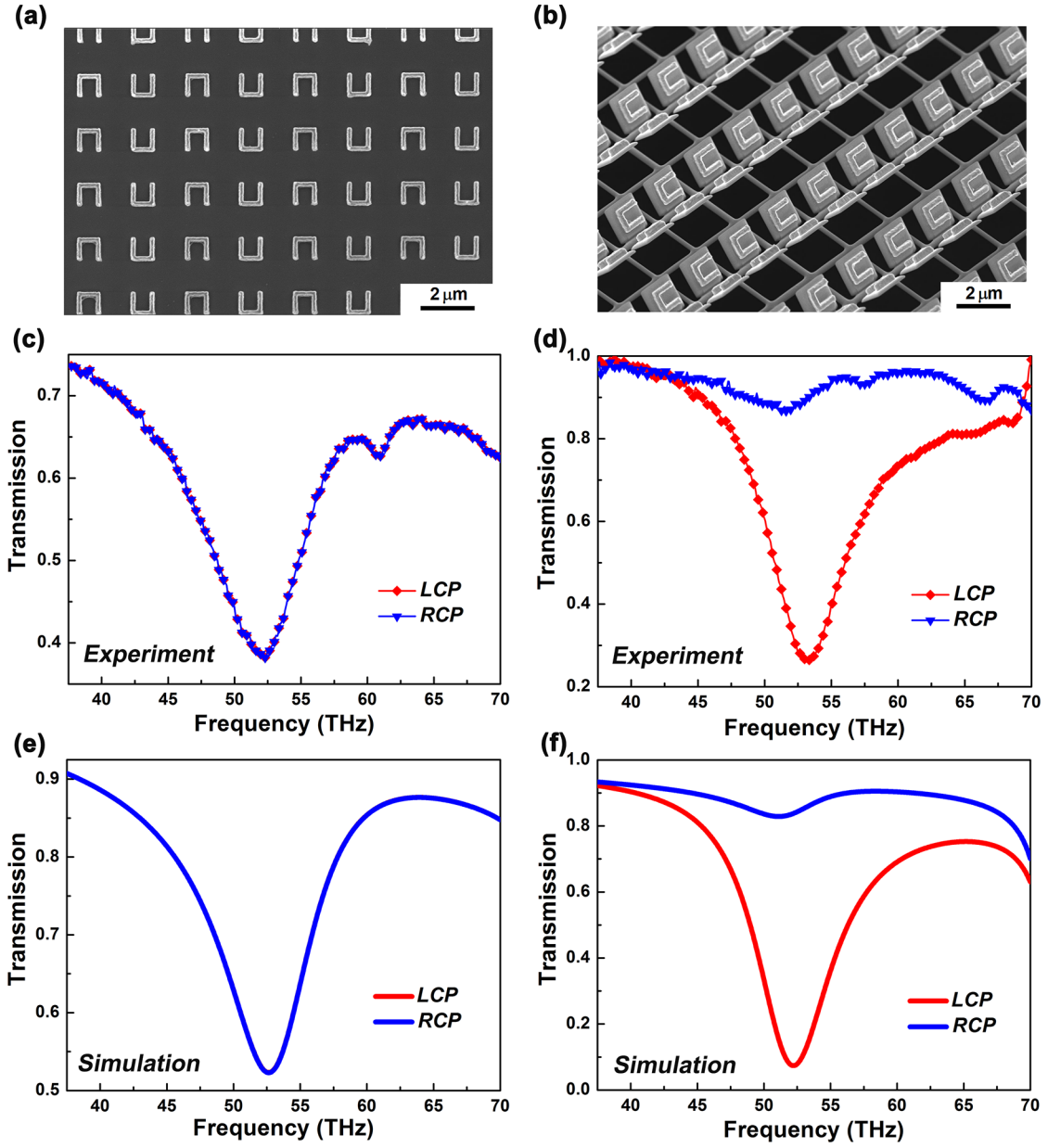

Figure 2. Experimental demonstration of spin selective transmission in 3D folded metasurfaces. SEM images of fabricated (a) unfolded planar metasurface consisting of antisymmetric SRRs and (b) 3D folded metasurface with the folding angle equal to 50°. Experimentally measured transmission spectra of the (c) unfolded metasurface and (d) 3D folded metasurface under the illumination of circularly polarized waves propagating along the *z*-axis. The blue (red) line refers to the incident polarization of RCP (LCP) light. Simulated transmission spectra of the (e) unfolded metasurface and (f) folded metasurface for circularly polarized light, which agree well with the measured transmission spectra.

the scanning electron microscope (SEM) image of the fabricated folded metasurface, with a magnified view of the structures shown in the inset. Very good uniformity of the structures across a sufficiently large area is achieved. The planar and folded metasurface devices are both characterized using Fourier transform infrared spectroscopy (FTIR) microscope with an achromatic quarter wave plates inserted into the beam path between a linear polarizer and the sample (with details summarized in the Methods section). In order to validate our design and optimize the functionality of the folded metasurface device, full-wave numerical simulations are performed by using commercially available CST Microwave Studio, which is based on the finite element method.

In general, the physical properties of a chiral medium are characterized by a magnetoelectric coupling between electric and magnetic fields along the same direction according to the Rosenfeld criterion.[40] The electromagnetic response of bianisotropic chiral media obeys the following constitutive relations[41−43]

$$\bar{D} = \bar{\bar{\varepsilon}}\bar{E} + \bar{\bar{\xi}}\bar{H} \tag{1}$$

$$B = \bar{\bar{\mu}}\bar{H} + \bar{\bar{\zeta}}\bar{E} \tag{2}$$

where $\bar{\bar{\varepsilon}}$, $\bar{\bar{\mu}}$, $\bar{\bar{\xi}}$, and $\bar{\bar{\zeta}}$ are 2 × 2 complex-valued matrices. For reciprocal materials, it can be shown that $\bar{\bar{\varepsilon}} = \bar{\bar{\varepsilon}}^{T}$, $\bar{\bar{\mu}} = \bar{\bar{\mu}}^{T}$, and $\bar{\bar{\xi}} = -\bar{\bar{\zeta}}^{T}$, where T represents for the transpose matrix. The actual form of $\bar{\bar{\xi}}$, which characterizes the magnetoelectric coupling effect between electric and magnetic fields, depends on the geometrical parameters of anisotropic inclusions. The chiral

DOI: 10.1021/acs.nanolett.8b04521
Nano Lett. XXXX, XXX, XXX−XXX

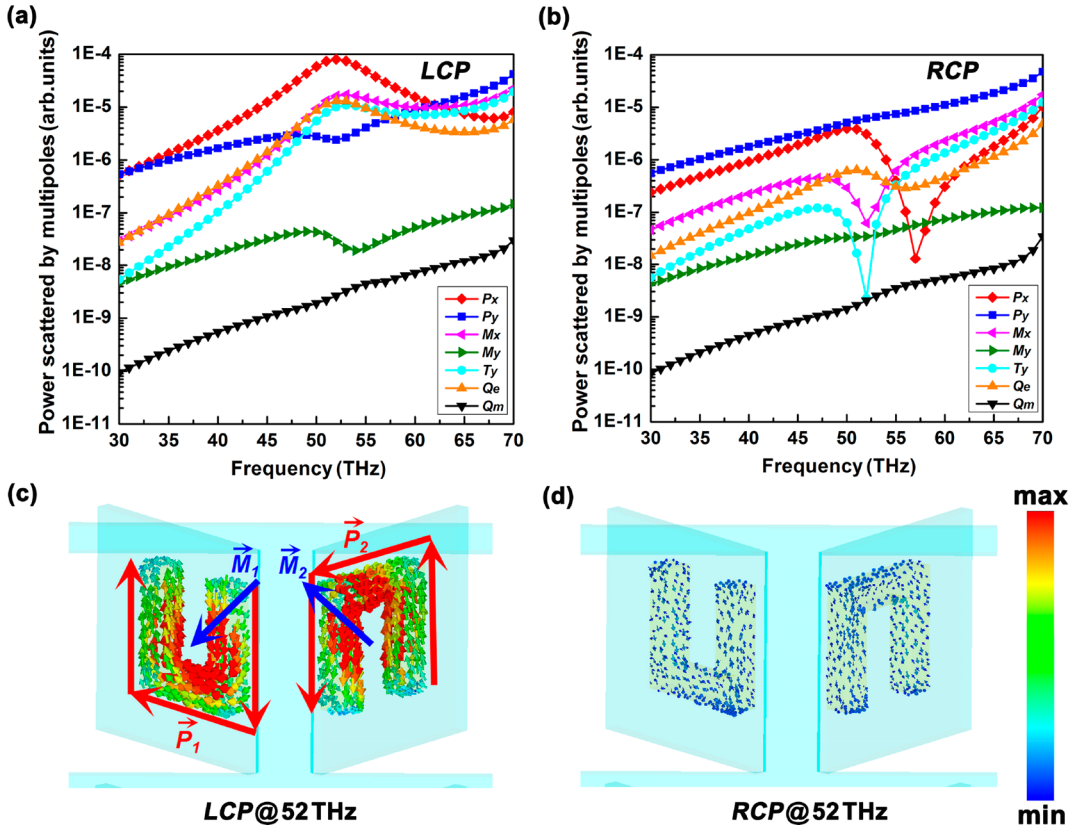

Figure 3. Multipole analysis and surface current distributions unraveling the underlying physical mechanism of the chiral optical response of the folded metasurfaces. Dispersion of scattered power for various multipole moments induced in the folded metasurface that contribute to the transmission spectra for the (a) LCP and (b) RCP incident light. Distributions of surface current for correspondingly chiral response at 52 THz for (c) LCP and (d) RCP incident light. The difference in the surface current oscillations on the structure indicates its intrinsic chiral-optical behavior due to different multipole excitations when illuminated with different spin states. The folded metasurface can support oblique magnetic dipoles that have a nonzero component in the direction of the in-plane electric moments.

parameter included in $\overline{\overline{\xi}}$ results in the breaking of the spin degeneracy of the two circularly polarized waves; i.e., the refractive index is distinct for the propagating LCP and RCP waves. In our scheme, the chiral parameter critically depends on the folding angle θ. By elaborately designing the geometrical parameters of the folded metasurface, the coupling between the electromagnetic multipoles excited in the folded metasurfaces can provide very strong chiral optical responses and spin selective transmission.

Parts a and b of Figure 2 display the SEM images of the as-fabricated planar metasurface and 3D folded metasurface, respectively, while the corresponding experimentally measured transmission properties for RCP and LCP incidence are shown in Figure 2c,d. Simulated transmission spectra of the planar and folded metasurface are also provided in Figure 2e,f, respectively. It is evident that the simulation results agree well with the measured data, where the slight difference in resonant strength primarily arises from imperfections in the fabrication process and dielectric material losses. As shown in Figure 2c,e, the fundamental inductive-capacitive resonance[44,45] of the antisymmetric SRR at around 52 THz is directly excited by either LCP or RCP incident light, and the transmission spectra measured for LCP and RCP light are nearly identical for the planar metasurface, which indicate that there is no intrinsic chirality for the unfolded metasurface. In contrast, when the metasurface is transformed into the folded configuration without any mirror symmetry, the intrinsic chirality of the folded metasurface leads to significantly distinct transmission spectra for LCP and RCP incident light, as the folded metasurface transmits most of the RCP incident light while the opposite circular polarization is largely blocked. Specifically, when LCP light impinges on the folded metasurfaces, a strong resonance occurs with a minimum transmission of 0.26, whereas the resonance is largely suppressed and maintains a high transmission of 0.91 for RCP incident light, as indicated in Figure 2d. These results suggest that the 3D folded metasurface supports spin selective transmission in the spectra range of interest. The difference between the transmission spectra of LCP and RCP tends to diminish far away from the resonance, indicating the significant role of the chiral response in achieving spin selective transmission. To quantitatively characterize the difference between the transmissions of the two spin states of incident light, the circular dichroism (CD = $|T_{RCP}| - |T_{LCP}|$) is further retrieved. A large CD up to 0.65 is experimentally achieved at the resonance frequency for the folded metasurface, while there exists no circular dichroism for the unfolded antisymmetric SRRs. It is worth noting that the sign of the circular dichroism can be reversed when the relative orientations of the folding SRR are interchanged, i.e., the transmittance of the LCP and RCP light can be reversed by changing the orientation of the folded SRRs.

In order to elucidate the underlying physics of the observed spin resolved characteristics of the folded metasurface, we quantitatively analyze the radiated powers of different

DOI: 10.1021/acs.nanolett.8b04521
Nano Lett. XXXX, XXX, XXX−XXX

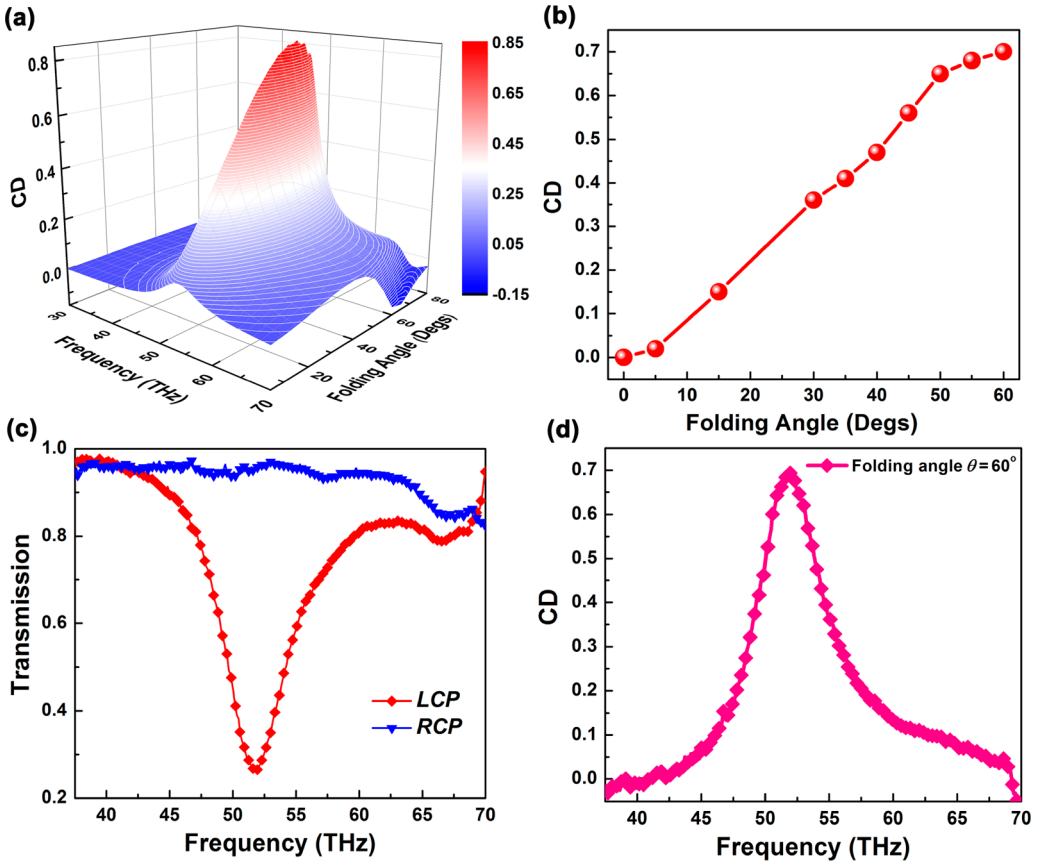

Figure 4. (a) Simulated CD spectra of the folded metasurface for a sweep of the folding angle from 5° to 80°. (b) Experimentally measured CD values at the chiral resonance frequency as a function of the folding angle. (c) Experimentally measured transmission spectra of the folded metasurface with folding angle $\theta = 60^{o}$ under the illumination of LCP and RCP light. (d) CD curve of the folded metasurface with folding angle $\theta = 60^{o}$.

multipole moments induced in the folded metasurface under excitation with LCP and RCP light, respectively, according to the general multipole scattering theory[38,39,46,47]

$$I = \frac{2\omega^4}{3c^3}|P|^2 + \frac{2\omega^4}{3c^3}|M|^2 + \frac{4\omega^5}{3c^4}(P\cdot T) + \frac{2\omega^6}{3c^5}|T|^2 + \frac{\omega^6}{5c^5}\sum|Q_{\alpha\beta}|^2 + \frac{\omega^6}{40c^5}\sum|M_{\alpha\beta}|^2 + O\left(\frac{1}{c^5}\right) \quad (3)$$

where P, M, T, $Q_{\alpha\beta}$, and $M_{\alpha\beta}$ are the electric dipole, magnetic dipole, toroidal dipole, electric quadrupole, and magnetic quadrupole, respectively, c is the speed of light in the vacuum and $\alpha, \beta = x, y, z$. Parts a and b of Figure 3 show the dispersion of radiation power for multipole moments calculated from the induced currents in the folded metasurface with LCP and RCP incident waves, respectively. The radiations of the folded metasurface under illumination of circularly polarized light with distinct spin states are significantly different. The total scattering efficiency of the folded metasurface with LCP incident light is more than 1 order of magnitude higher than that of with RCP incident light, which agrees well with the transmission spectra. For the LCP incident light, the x-components of the electric dipole, magnetic dipole, toroidal dipole, and the electric quadrupole dominate over all the other multipoles and exhibit maximum radiated power at the resonance frequency. Contrary to the LCP incidence, in which the electric dipole moment has the dominant radiation intensity, the magnitude of the electric dipole moment for RCP incidence is about 13 times smaller than that for LCP incident light. Parts c and d of Figure 3 depict the surface current distributions on the folded metasurface at the resonant frequency for LCP and RCP incident light, respectively. An LCP incident wave induces strong circular current loops on the antisymmetric SRRs, which means that the LCP incident wave interacts strongly with the folded metasurface, while for an RCP wave the current intensity is much smaller. The interaction between the folded metasurface and RCP wave is negligibly weak, and thus the RCP wave can propagate through the sample with high transmittance. Benefiting from photon-spin dependent surface current distributions in the folded metasurface, distinct responses in absorption and scattering to different spins of circularly polarized light result in the strong dichroism. Specifically, as revealed by the surface current distributions in folded metasurface with LCP incidence, antiphase oscillations of current loops configuration in the antisymmetrical folded SRRs lead to the enhancement of the electric and magnetic dipole components oriented in the x-direction. The effective x-components of the electric and magnetic dipoles can be mathematically expressed as $|\vec{P}_{\mathrm{eff},x}| = |\vec{P}_1|\cdot\cos\theta + |\vec{P}_2|\cdot\cos\theta$ and $|\vec{M}_{\mathrm{eff},x}| = |\vec{M}_1|\cdot\sin\theta + |\vec{M}_2|\cdot\sin\theta$, respectively. Consequently, the parallel configuration of the x-components of electric and magnetic dipole moment leads to strong cross-coupling between electric and magnetic fields, contributing to the chiral optical response of the folded metasurface. Moreover, the individual magnetic moments induced by circular currents in the antisymmetric SRRs are

DOI: 10.1021/acs.nanolett.8b04521
Nano Lett. XXXX, XXX, XXX−XXX

nearly opposite, forming a head-to-tail configuration of the magnetic moments, which gives rise to an in-plane toroidal dipole moment oriented along the y-axis (T_y).[39] Therefore, both the strong toroidal dipole and electric quadrupole induced in the antisymmetric structures also play important roles in the intrinsic chiral response of the folded metasurface. As a result, the strong dichroism of the folded metasurface mainly arises from the electric-magnetic dipole coupling as well as contribution from the electric quadrupole and toroidal dipole moments.

Chiral media with arbitrarily controllable CD is highly desired in various applications such as polarization modulation and chiral optical imaging. The modulation of CD generally requires elaborately tailoring multiple geometrical parameters of conventional chiral metamaterials. Interestingly, our folded metasurface provides a precise and effective method to manipulate the CD via the folding angle of SRRs while keeping the other structural parameters fixed. To optimize the chiral optical properties, the effect of the folding angle on the evolution of CD performance is further investigated by tailoring the folding angle of SRRs. The simulated CD spectra as a function of folding angle θ are presented in Figure 4a. For a clear visualization and demonstration, the experimentally measured CD of the folded metasurface at the chiral responses is also provided, as shown in Figure 4b. The folding angle is limited to 60° in the experiment to avoid damage of the metal patterns by the focused ion beam. The simulated and experimental results clearly show that the chiral characteristics of the folded metasurface experiences a dramatic modification with varied folding angle θ. The frequency of the transmission peak slightly red shifts with the increase of the folding angle. With the folding angle gradually increased from θ = 5° to 60°, the CD tends to increase dramatically over the spectrum of interest as a result of gradually improved impedance match and enhanced coupling strength between the antisymmetric SRRs. Intriguingly, it can be observed that the chiral optical response is most pronounced when the folding angle is 60°, where the experimental measured maximum CD at chiral resonance can reach up to 0.7 with >90% transmission of the selected circularly polarized light (see Figure 4c,d). In this case, the electromagnetic coupling is strongest because the electric dipole (P_x) and magnetic dipole (M_x) are of comparable magnitude. The remarkable CD resonance in Figure 4d further confirm a highly efficient spin selective transmission and a significant optical chirality, which are in good accordance with simulations. However, further increasing the folding angle from 60° to 80°, the chiral response and the magnitude of CD is gradually weakened and finally collapsed once the SRRs is conductively connected. This is due to the attenuated excitation efficiency of the circular currents in the antisymmetric SRRs, and thus the multipole components as well as electric-magnetic coupling are degraded. Through controlling the folding angle, the intrinsic chirality of the folded metasurface can be effectively modulated to make the spin selective transmission controllable. Compared with the natural chiral materials and conventional planar chiral metamaterials, the folded metasurfaces possess strong 3D intrinsic chirality and a greater degree of freedom in CD control.

Providing spin selective transmission functionality while retaining an ultrathin, simple and compact design makes the folded metasurfaces highly promising for various practical applications. Although here we have focused on folded metasurfaces operating within the technologically relevant infrared frequencies, the proposed scheme and fabrication techniques can be readily extended to shorter or longer wavelengths such as optical and terahertz frequencies by selecting a membrane with appropriate permittivity and tailoring the geometrical parameters. For instance, a folded metasurface operating in the visible regime can be achieved by scaling down the size of folded structures and by replacing the SiN_x membrane by low-dielectric-constant materials. The folded metasurface may also find valuable applications in chiral biomolecule identification and drug analysis by detecting the CD to determine the configuration of molecules.

Conclusions. In conclusion, we have experimentally demonstrated a relatively simple and apparently robust technique for engineering 3D strong intrinsic chirality by novel folded metasurfaces, which is promising for compact optical devices. The giant intrinsic chirality is engineered by antisymmetric spatial arrangement of the neighboring SRRs such that the mutual interactions between the SRRs lead to remarkable distinction in the transmission spectra of LCP and RCP light. By tailoring the folding angle of the constituent SRRs, the intrinsic chirality can be precisely engineered and a giant CD as high as 0.7 is experimentally achieved. Furthermore, the concept of folded metasurface represents a unique way to implement and modulate the intrinsic chiral responses, to develop miniature circular polarizer, polarization transformers, stealth technology, and CD spectroscopy.

Methods. Nanofabrication. First, poly(methyl methacrylate) (PMMA) resist was spin-coated on the 100 nm thick low-stress SiN_x window (Shanghai NTI Co., Ltd.) and baked at 180 °C for 1 min, after which the metasurface patterns were defined on the resist layer by electron beam lithography. Subsequently, a 200 nm thick gold film was deposited onto the samples using the thermal evaporation method followed by an acetone lift-off procedure to obtain metasurface array. After that, a 20 nm aluminum conductive layer was deposited onto the planar metasurfaces as a conductive layer by thermal evaporation. Then a focused-ion-beam system (Helios 600i, FEI) was utilized to cut the SiN_x film into sheets, and the structures folded up naturally by the ion-implantation induced stress via continuously scanning the bottom edge of the SiN_x sheets. The acceleration voltage of focused gallium ions is 30 kV, and the ion beam current is 40 pA. Finally, the aluminum conductive layer was removed by wet etching in NaOH solution and thus the folded metasurfaces are implemented. Each sample has a 100 × 100 μm^2 pattern area. It is worth mentioning that the electron beam lithography process can be alternatively replaced by the ultraviolet lithography (UV) or extreme ultraviolet lithography (EUV), which are compatible with the traditional CMOS fabrication platform and suitable for mass production. The folding processes are programmable and automatically completed by the focused-ion-beam system.

Optical Characterization. Transmission spectra were measured using a Fourier-transform infrared spectrometer (Vertex 80, Bruker) coupled to a confocal microscope (Hyperion 2000 IR), which was equipped with a × 15, NA= 0.4 objective lens and a liquid nitrogen cooled mercury cadmium telluride (MCT) detector. A ZnSe polarizer was used to polarize the incident electromagnetic field. Transmission measurements for circularly polarized light are carried out by inserting a custom ordered Mid-IR achromatic quarter wave plate with a retardation of $\lambda/4$ (B. Halle Nachfl. GmbH) into the beam path between a linear polarizer and the sample. All the spectra were measured with a resolution of 4 cm^{-1} and 128

DOI: 10.1021/acs.nanolett.8b04521
Nano Lett. XXXX, XXX, XXX−XXX

scans. All transmission spectra were normalized with respect to air.

Numerical Simulations. The numerical simulations were performed by using the frequency domain solver of the commercial software package CST Microwave Studio, which implements a finite element method. Unit cell boundary conditions in the $x-y$ plane and Floquet ports in the z direction were employed, and the circular polarized eigenwaves were applied directly. At least five mesh steps per wavelength were used to ensure the accuracy of the calculated results. The refractive index of the SiN_x substrate was set to be 2.2. Realistic material parameters were used for describing gold's lossy properties with an electric conductivity of 4.561×10^7 S m^{-1}. The surface current distributions were obtained using an H-field/surface current monitor.

AUTHOR INFORMATION

Corresponding Authors

*E-mail: s.zhang@bham.ac.uk.
*E-mail: jjli@iphy.ac.cn.
*E-mail: czgu@iphy.ac.cn.

ORCID

Shengyan Yang: 0000-0003-0667-3743
Shuang Zhang: 0000-0003-4556-2333
Junjie Li: 0000-0002-1508-9891
Changzhi Gu: 0000-0002-2689-2807

Author Contributions

S.Y. and S.Z conceived the idea and designed the experiment. S.Y., Z.L., A.J. and H.Y. fabricated the devices. S.Y., Z.L, and S.H. performed the optical measurements. S.Y. and Z.L. conducted the calculations and simulations. S.Y. and S.Z. prepared the manuscript. S.Z., J.L., and C.G. supervised the overall project. All the authors analyzed the data and discussed the results. S.Y. and Z.L. contributed equally to this work.

Notes

The authors declare no competing financial interest.

ACKNOWLEDGMENTS

This work is supported by the National Key Research and Development Program of China under Grant Nos. 2016YFA0200400 and 2016YFA0200800; the National Natural Science Foundation of China under Grants Nos. 91323304, 11674387, 11504414, 11574369, 11574385, 11574368, 11434017, and 61390503; Strategic Priority Research Program and Key Research Program of Frontier Sciences, CAS, Grant Nos. XDB07020200 and QYZDJ-SSW-SLH042; European Research Council Consolidator Grant (TOPOLOGICAL).

REFERENCES

(1) Togan, E.; Chu, Y.; Trifonov, A. S.; Jiang, L.; Maze, J.; Childress, L.; Dutt, M. V. G.; Sørensen, A. S.; Hemmer, P. R.; Zibrov, A. S.; Lukin, M. D. *Nature* **2010**, *466*, 730−734.
(2) Wagenknecht, C.; Li, C.-M.; Reingruber, A.; Bao, X.-H.; Goebel, A.; Chen, Y.-A.; Zhang, Q.; Chen, K.; Pan, J.-W. *Nat. Photonics* **2010**, *4*, 549−552.
(3) Greenfield, N. *J. Nat. Protoc.* **2007**, *1*, 2876−2890.
(4) Ranjbar, B.; Gill, P. *Chem. Biol. Drug Des.* **2009**, *74*, 101−120.
(5) Farshchi, R.; Ramsteiner, M.; Herfort, J.; Tahraoui, A.; Grahn, H. T. *Appl. Phys. Lett.* **2011**, *98*, 162508.
(6) Hendry, E.; Carpy, T.; Johnston, J.; Popland, M.; Mikhaylovskiy, R. V.; Lapthorn, A. J.; Kelly, S. M. *Nat. Nanotechnol.* **2010**, *5*, 783−787.
(7) Zhao, Y.; Askarpour, A. N.; Sun, L.; Shi, J.; Li, X.; Alu, A. *Nat. Commun.* **2017**, *8*, 14180.
(8) Tinoco, I.; Cantor, C. R. *Application of Optical Rotatory Dispersion and Circular Dichroism to the Study of Biopolymers*; John Wiley & Sons, 2006.
(9) Jaggard, D. L.; Mickelson, A. R.; Papas, C. H. *Appl. Phys.* **1979**, *18*, 211−216.
(10) Barron, L. D. *Molecular Light Scattering and Optical Activity*; Cambridge University Press, 2004.
(11) Valev, V. K.; Baumberg, J. J.; Sibilia, C.; Verbiest, T. *Adv. Mater.* **2013**, *25*, 2517.
(12) Papakostas, A.; Potts, A.; Bagnall, D. M.; Prosvirnin, S. L.; Coles, H. J.; Zheludev, N. I. *Phys. Rev. Lett.* **2003**, *90*, 107404.
(13) Kuwata-Gonokami, M.; Saito, N.; Ino, Y.; Kauranen, M.; Jefimovs, K.; Vallius, T.; Turunen, J.; Svirko, Y. *Phys. Rev. Lett.* **2005**, *95*, 227401.
(14) Zhao, R.; Zhang, L.; Zhou, J.; Koschny, T.; Soukoulis, C. M. *Phys. Rev. B: Condens. Matter Mater. Phys.* **2011**, *83*, 035105.
(15) Zhou, J.; Chowdhury, D. R.; Zhao, R.; Azad, A. K.; Chen, H.-T.; Soukoulis, C. M.; Taylor, A. J.; O'Hara, J. F. *Phys. Rev. B: Condens. Matter Mater. Phys.* **2012**, *86*, 035448.
(16) Fedotov, V. A.; Mladyonov, P. L.; Prosvirnin, S. L.; Rogacheva, A. V.; Chen, Y.; Zheludev, N. I. *Phys. Rev. Lett.* **2006**, *97*, 167401.
(17) Xu, H. X.; Wang, G. M.; Qi, M. Q.; Cai, T.; Cui, T. *Opt. Express* **2013**, *21*, 24912−24921.
(18) Hannam, K.; Powell, D. A.; Shadrivov, I. V.; Kivshar, Y. S. *Phys. Rev. B: Condens. Matter Mater. Phys.* **2014**, *89*, 125105.
(19) Collins, J. T.; Kuppe, C.; Hooper, D. C.; Sibilia, C.; Centini, M.; Valev, V. K. *Adv. Opt. Mater.* **2017**, *5*, 1700182.
(20) Plum, E.; Liu, X. X.; Fedotov, V. A.; Chen, Y.; Tsai, D. P.; Zheludev, N. I. *Phys. Rev. Lett.* **2009**, *102*, 113902.
(21) Plum, E.; Fedotov, V. A.; Zheludev, N. I. *Appl. Phys. Lett.* **2016**, *108*, 141905.
(22) Pendry, J. B. *Science* **2004**, *306*, 1353.
(23) Zhang, S.; Park, Y. S.; Li, J.; Lu, X.; Zhang, W.; Zhang, X. *Phys. Rev. Lett.* **2009**, *102*, 023901.
(24) Plum, E.; Zhou, J.; Dong, J.; Fedotov, V. A.; Koschny, T.; Soukoulis, C. M.; Zheludev, N. I. *Phys. Rev. B: Condens. Matter Mater. Phys.* **2009**, *79*, 035407.
(25) Zhou, J.; Dong, J.; Wang, B.; Koschny, T.; Kafesaki, M.; Soukoulis, C. M. *Phys. Rev. B: Condens. Matter Mater. Phys.* **2009**, *79*, 121104.
(26) Gansel, J. K.; Thiel, M.; Rill, M. S.; Decker, M.; Bade, K.; Saile, V.; Wegener, M. *Science* **2009**, *325*, 1513.
(27) Kaschke, J.; Blume, L.; Wu, L.; Thiel, M.; Bade, K.; Yang, Z.; Wegener, M. *Adv. Opt. Mater.* **2015**, *3*, 1411−1417.
(28) Esposito, M.; Tasco, V.; Todisco, F.; Cuscuna, M.; Benedetti, A.; Sanvitto, D.; Passaseo, A. *Nat. Commun.* **2015**, *6*, 6484.
(29) Esposito, M.; Tasco, V.; Cuscunà, M.; Todisco, F.; Benedetti, A.; Tarantini; Giorgi, I. M. D.; Sanvitto, D.; Passaseo, A. *ACS Photonics* **2015**, *2*, 105−114.
(30) Kosters, D.; Hoogh, A.; Zeijlemaker, H.; Acar, H.; Rotenberg, N.; Kuipers, L. *ACS Photonics* **2017**, *4*, 1858−1863.
(31) Zhang, S.; Zhou, J.; Park, Y.- S.; Rho, J.; Singh, R.; Nam, S.; Azad, A. K.; Chen, H.-T.; Yin, X.; Taylor, A. J.; Zhang, X. *Nat. Commun.* **2012**, *3*, 942.
(32) Decker, M.; Ruther, M.; Kriegler, C. E.; Zhou, J.; Soukoulis, C. M.; Linden, S.; Wegener, M. *Opt. Lett.* **2009**, *34*, 2501−2503.
(33) Zhao, Y.; Belkin, M. A.; Alu, A. *Nat. Commun.* **2012**, *3*, 870.
(34) Helgert, C.; Pshenay-Severin, E.; Falkner, M.; Menzel, C.; Rockstuhl, C.; Kley, E.; Tunnermann, A.; Lederer, F.; Pertsch, T. *Nano Lett.* **2011**, *11*, 4400−4404.
(35) Hentschel, M.; Schäferling, M.; Weiss, T.; Liu, N.; Giessen, H. *Nano Lett.* **2012**, *12*, 2542−2547.
(36) Cui, Y.; Kang, L.; Lan, S.; Rodrigues, S.; Cai, W. *Nano Lett.* **2014**, *14*, 1021−1025.
(37) Hentschel, M.; Ferry, V. E.; Alivisatos, A. P. *ACS Photonics* **2015**, *2*, 1253−1259.

DOI: 10.1021/acs.nanolett.8b04521
Nano Lett. XXXX, XXX, XXX−XXX

(38) Liu, Z.; Du, S.; Cui, A.; Li, Z.; Fan, Y.; Chen, S.; Li, W.; Li, J.; Gu, C. *Adv. Mater.* **2017**, *29*, 1606298.
(39) Yang, S.; Liu, Z.; Jin, L.; Li, W.; Zhang, S.; Li, J.; Gu, C. *ACS Photonics* **2017**, *4*, 2650−2458.
(40) Rosenfeld, L. Z. *Eur. Phys. J. A* **1929**, *52*, 161.
(41) Priou, A.; Sihvola, A.; Tretyakov, S.; Vinogradov, A. *Advances in Complex Electromagnetic Materials*; Kluwer Academic Publishers, 1997.
(42) Bayatpur, F.; Amirkhizi, A. V.; Nemat-Nasser, S. *IEEE Trans. Microwave Theory Tech.* **2012**, *60*, 1126−1135.
(43) Chen, X.; Wu, B.-I.; Kong, J. A.; Grzegorczyk, T. M. *Phys. Rev. E* **2005**, *71*, 046610.
(44) Yang, S.; Liu, Z.; Xia, X.; E, Y.; Tang, C.; Wang, Y.; Li, J.; Wang, L.; Gu, C. *Phys. Rev. B: Condens. Matter Mater. Phys.* **2016**, *93*, 235407.
(45) Yang, S.; Tang, C.; Liu, Z.; Wang, B.; Wang, C.; Li, J.; Wang, L.; Gu, C. *Opt. Express* **2017**, *25*, 15938.
(46) Kaelberer, T.; Fedotov, V. A.; Papasimakis, N.; Tsai, D. P.; Zheludev, N. I. *Science* **2010**, *330*, 1510.
(47) Huang, Y.-W.; Chen, W. T.; Wu, P. C.; Fedotov, V.; Savinov, V.; Ho, Y. Z.; Chau, Y.-F.; Zheludev, N. I.; Tsai, D. P. *Opt. Express* **2012**, *20*, 1760.

DOI: 10.1021/acs.nanolett.8b04521
Nano Lett. XXXX, XXX, XXX−XXX